



“BABEȘ-BOLYAI” UNIVERSITY  
CLUJ-NAPOCA

FACULTY OF PHYSICS

Physical properties of some transition  
metal oxides.

Scientific coordinator  
Prof.Dr. Romulus Tetean

PhD. Student  
Adrian Vladescu

Cluj-Napoca 2012



Proiect finanțat de  
UNIUNEA EUROPEANĂ



MINISTERUL MUNCII, FAMILIEI ȘI  
PROTECȚIEI SOCIALE  
AMPOSORUJ



FONDUL SOCIAL EUROPEAN  
POSDRU  
2007-2013



INSTRUMENTE STRUCTURALE  
2007-2013



MINISTERUL EDUCAȚIEI,  
CERCETĂRII ȘI INOVĂRII  
OPROSERU



UNIVERSITATEA BABEȘ-BOLYAI  
CLUJ-NAPOCA



# Contents

<b>1. INTRODUCTION</b>	<b>1</b>
<b>2. THE PEROVSKITIC STRUCTURE IN COBALTITES.</b>	<b>2</b>
2.1. Fundamental properties	3
2.2. Magnetic properties	3
2.3. Transport properties	4
<b>3. EXPERIMENTAL TECHNIQUES</b>	<b>5</b>
<b>3.1. Preparation methods</b>	<b>5</b>
3.1.1. Solid state reaction	5
3.1.2. Sol-gel method	5
3.1.3. Mechanical alloying	5
<b>3.2. Structural analysis</b>	<b>6</b>
3.2.1. X-ray Diffraction	6
3.2.2. SEM (Scanning Electron Microscopy)	6
<b>3.3. Magnetic and transport investigations</b>	<b>7</b>
3.3.1. VSM (Vibrating Sample Magnetometer)	7
3.3.2. Four-probe method	7
3.3.3. $\mu$ SR (Muon Spin Rotation/Relaxation/Resonance)	7
<b>4. RESULTS</b>	<b>8</b>
<b>4.1. The <math>\text{Pr}_{1-x}\text{Sr}_x\text{CoO}_3</math> system</b>	<b>8</b>
4.1.1. Sample preparation	8
4.1.2. Structural analysis	8
4.1.3. Magnetic and transport properties of the $\text{Pr}_{1-x}\text{Sr}_x\text{CoO}_3$ compound	9
4.1.4. Preliminary Conclutions	13
<b>4.2. The <math>\text{Pr}_{0.7}(\text{Ca}_{1-x}\text{Sr}_x)_{0.3}\text{CoO}_3</math> system</b>	<b>14</b>
4.2.1. Sample preparation	14

4.2.2.	Structural analysis	14
4.2.3.	Magnetic and transport properties of the $\text{Pr}_{0.7}(\text{Ca}_{1-x}\text{Sr}_x)\text{CoO}_3$ compound	14
4.2.4.	Preliminary Conclusions	18
<b>4.3.</b>	<b>The <math>\text{Nd}_{1-x}\text{Sr}_x\text{CoO}_3</math> system</b>	<b>18</b>
4.3.1.	Sample preparation	18
4.3.2.	Structural analysis	18
4.3.3.	Magnetic properties and transport properties	19
4.3.4.	Preliminary conclusions	20
<b>4.4.</b>	<b>The <math>\text{La}_{1.2}\text{R}_{0.2}\text{Ca}_{1.6}\text{Mn}_2\text{O}_7</math> compounds (with R = Nd, Ho, Yb)</b>	<b>21</b>
4.4.1.	Sample preparation	21
4.4.2.	Structural analysis	21
4.4.3.	Magnetic measurements	21
4.4.4.	Preliminary Conclusions	23
	<b>Conclusions</b>	<b>23</b>
	<b>Selected References</b>	<b>26</b>
	<b>List of Publications</b>	<b>27</b>

**Keywords:** Cobaltites and manganites based compounds; X-ray diffraction; Magnetic measurements;  $\mu\text{SR}$  measurements, Magnetocaloric effect, Magnetoresistance, Transition temperature.

## 1. Introduction

The cobaltites with perovskite-type structure have been lately studied with greater interest because of their specific properties, which make them promising materials for use in solid oxide fuel cell, chemical reactors, gas separation membranes and many other applications [1].

The magnetic structures, especially of the layered cobaltite compounds with oxygen content of 5.5 per unit formula, are still under debate. The determination of the magnetic structure is a complex task, because, contrary to other materials, the Co ion in these materials can be in different spin states. The ratio between different Co ionic configurations is determined by oxygen content, following the charge neutrality condition.

Regarding electronic transport properties, the cobaltites, depending on oxygen content, either belongs to the class of metals with poor conductivity or semiconductors (with the exception of the metallic  $\text{SrCoO}_3$  compounds).

The Mn-based perovskites, exhibiting MR/CMR have been extensively studied in the last few years [2, 3]. More recently, the focus has shifted to some other extended valence transition metal compounds, such as Co- and Fe-based perovskite compounds [4–6].

More recently, the double-layered manganites belonging to the Ruddelsden–Popper series ( $n=2$ ) have been studied for their colossal magnetoresistance and intricate magnetic structure [7, 8]. Colossal magnetoresistance was first observed in these layered phases by Moritomo et al. in  $\text{Sr}_{2-x}\text{La}_{1+x}\text{Mn}_2\text{O}_7$  ( $x=0.2$ ), which has a Curie temperature for three-dimensional ferromagnetic ordering of 126 K [7].

The thesis is organized in 4 Chapters, followed by the general conclusions. Chapter 1 is a short introduction containing information on the history and development of transition metal oxides. Chapter 2 contains a brief theoretical introduction into the structural, magnetic and transport properties of these kind of materials. The third chapter contains information about the experimental techniques we used in order to prepare and analyze the samples. Chapter four contains the experimental results on  $\text{Pr}_{1-x}\text{Sr}_x\text{CoO}_3$ ,  $\text{P}_{0.7}(\text{Ca}_{1-x}\text{Sr}_x)_{0.3}\text{CoO}_3$ ,  $\text{Nd}_{1-x}\text{Sr}_x\text{CoO}_3$ , for different values of  $x$ , and  $\text{La}_{1.2}\text{R}_{0.2}\text{Ca}_{1.6}\text{Mn}_2\text{O}_7$  (where  $\text{R} = \text{Nd}, \text{Sm}, \text{Ho}$  or  $\text{Yb}$ ) systems.

## 2. The perovskitic structure in cobaltites.

The perovskite structure is adopted by many oxides that have the chemical formula  $ABO_3$ . In the idealized cubic unit cell of such a compound, type A atom sits at cube corner positions  $(0, 0, 0)$ , type B atom sits at body centre position  $(1/2, 1/2, 1/2)$  and oxygen atoms sit at face centered positions  $(1/2, 1/2, 0)$ . (Figure 2.1)

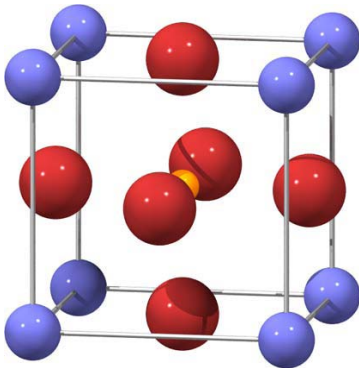


**Figure 2.1.** Cubic perovskite unit cell.[10]

**Table 2.1.** Atomic positions in cubic perovskites

Site	Location	Co-ordinates
A cation	(2a)	$(0, 0, 0)$
B cation	(2a)	$\left(\frac{1}{2}, \frac{1}{2}, \frac{1}{2}\right)$
O anion	(6b)	$\left(\frac{1}{2}, \frac{1}{2}, 0\right)\left(\frac{1}{2}, 0, \frac{1}{2}\right)\left(0, \frac{1}{2}, \frac{1}{2}\right)$

Using X-ray diffraction and neutron scattering techniques, detailed studies were possible on rare earth perovskites. Many early studies reported that the perovskites showed mainly cubic or pseudo cubic structure, but as work on these systems continued, the number of proposed symmetries increased.

As the measurement techniques improved, it was possible to more precisely determine the structure of some of the perovskites, which were then used as basis for subsequent modeling. Many of the materials exhibit the orthorhombic  $Pnma$  distorted structure at room temperature. A more pronounced distortion of the structure is possible and it will result in a rhomboedral structure having the  $R3c$  space group.

Any of the trivalent 3d cations can substitute partially for manganese. The main effects of the various substitutions are to vary the number of electrons in the 3d band and to alter the interatomic distances and bond angles. The mixed-valence manganites can exhibit magnetic order, charge order and orbital order.[9]

From a chemical point of view, the system is characterized by the wide range of cations, which will occupy the body centered positions of the cubic cell. The ideal cubic

structure is distorted by the differences in size between the cations and, the Jahn-Teller effect will appear. The distorted structures are frequently orthorhombic.

## **2.1. Fundamental properties**

In a perovskite structures, the two most important parameters, used to a considerable extent to modify its chemical composition are, the band filling (or doping level) and the bandwidth (or electron hopping interaction).

Both the parameters control the kinetic energy of the conduction electrons which not only governs the metal-insulator phenomena but also the competing magnetic interactions, i.e. ferromagnetic vs. antiferromagnetic, in the perovskite. [11]

Another important feature in the perovskite and related structures is that the compounds are quite suitable for the carrier-doping procedure (filling control) since the structure is very robust against the chemical modification on the A-site.

## **2.2. Magnetic properties**

If the interactions between the magnetic moments are strong enough range magnetic order may set in. In the case of 3d metal oxides, long range order is caused by the exchange interactions, which are basically of electrostatic origin.

The double exchange interaction correlates magnetic and electronic properties of a material. In cobaltites, double exchange can be introduced by decreasing oxygen content, introducing  $\text{Co}^{4+}$  at the place of  $\text{Co}^{3+}$  ions due to charge neutrality. This leads to two degenerate electronic states. Zener showed [12, 13] that a magnetic interaction leads to lifting of the degeneracy of these two states by creating two resonant wave functions. Double exchange associates the appearance of ferromagnetic coupling of the localized magnetic moments (in the  $t_{2g}$  energy level) to the delocalization of an  $e_g$  electron.

Because in many magnetic oxides, the magnetic ions are not close enough, it will no longer be possible to explain the magnetic coupling using the DE mechanism. Additionally, the ions carrying the magnetic moments are often separated by non-magnetic anions, such as oxygen.

Kramers and later Anderson proposed a mechanism called superexchange. [14, 15, 16] For this kind of mechanism the magnetic moments of magnetic cations are coupled indirectly through intermediate anions. The superexchange interaction is based on the

minimization of energy cost for the transfer of a virtual electron from the full p shell of the oxygen ion to the excited states of the neighboring magnetic Co ions.

3d transition metal ions are special because their d orbitals are only partially filled. In the case of  $\text{Co}^{3+}$ , only 6 electrons occupy orbital states instead of the maximum possible 10. For a weak crystal field the levels are filled according to Hund's rule (obeying the Pauli principle), which requires that the total spin is maximized.

#### *Magnetocaloric effect*

MCE is an isothermal magnetic entropy change or an adiabatic temperature change of a magnetic material upon application of a magnetic field. The compounds which undergo temperature driven paramagnetic to ferromagnetic transitions show relatively large "negative" MCE, in which the isothermal magnetic entropy changes are negative. [17–19]

Although perovskite *cobaltites* have received less attention than manganites, these materials have been the subject of considerable interest due to prospects of their use as magnetic media, cathode materials, etc.

### **2.3. Transport properties**

When the 3d orbitals of the metal overlap with the 2p orbitals of the oxygen in transition metal (TM) oxides, and form energy bands, they should lead to metallic conductivity. However, the transition metal ions are relatively small (especially the 3d variety) and the angle of the TM-O-TM is usually tilted, which leads to narrow energy bands. Additionally the Coulomb repulsion  $U$  between the electrons tends to keep the electrons localized, resulting in insulating properties. An approximation which is used to describe the transition metals is the Mott-Hubbard model, in which the repulsion between electrons is only considered when they are on the same atom [20].

For disordered systems with localized states (narrow bandwidth) the electron motion can be explained on the basis of Mott variable range hopping (VRH). In the hopping process the energy difference is always provided by a phonon. The hopping probability can become so small that transitions to states further away in distance, costing less energy, can become more likely.

#### *Magnetoresistance*

Although discovered in 1856 by William Thomson, anisotropic magnetoresistance phenomenon only recently found applications in magnetic field sensors. Anisotropic

magnetoresistance is the difference in local resistivity of a material depending on the circulating magnetic current parallel or perpendicular to the direction of local magnetization.

Magnetoresistance is basically the property of a material to change its electrical resistivity when an external magnetic field is applied.[21]

### **3. Experimental Techniques**

#### **3.1. Preparation methods**

##### **3.1.1. Solid state reaction**

A solid material with new properties can be obtained using the solid state reaction between some solid predecessors or transformations in solid state of the same material.

A very important aspect of the materials obtained by solid state reaction is that they have a considerable amount of pores. [22]

*Solid state sintering* takes place usually in monophasic systems and three stages can be observed through out the process.

- the appearance of the so called “inter-granular necks”
- growth of the inter-granular necks takes place
- in the third the diffusion length is bigger there for the modifications in the material structure are slower and smaller.

The diffusion and recrystallisation are the dominant mechanisms in high temperature sinterisation.[22]

##### **3.1.2. Sol-gel method**

The sol-gel process is a wet-chemical technique (a.k.a. chemical solution deposition) widely used recently in the fields of materials science and ceramic engineering.[23, 24]

This method is used primarily for the fabrication of materials (typically a metal oxide) starting from a chemical solution which acts as the precursor for an integrated network (or *gel*) of either discrete particles or network polymers.

##### **3.1.3. Mechanical alloying**

Being among the latest technique for obtaining magnetic materials, mechanical milling allows us to obtain microstructures with specific magnetic properties. The powders of the materials are placed in bowls together with balls for grinding process. To avoid oxidation the

bowls are usually loaded with powders of the materials in different atmosphere (argon, helium, nitrogen) or vacuum.

In the mechanical grinding process take place fragmentation (up to nanometric scale) and merge between different starts elements and in this way can be obtained nanocomposite materials.

## **3.2. Structural analysis**

### **3.2.1. X-ray Diffraction**

The major determinants of the structure of a material and thus of its properties are its constituent chemical elements and the way in which it has been processed into its final form. These characteristics, taken together and related through the laws of thermodynamics, govern a material's microstructure, and thus its properties.

In order to do such a characterization a source of rays and a detector are required. One of the obstacles is that the atoms are too small to be observed by use of visible light, which can have wavelengths in the range from  $\sim 4000$  to  $\sim 7000$  Å. The problem is solved with the use of X-ray because they are short wave electromagnetic radiation and thus permit the observation of individual atoms.

In our laboratory we used for the X Ray diffractions the Bruker Advance D8 AXS Diffractometer

### **3.2.2. SEM (Scanning Electron Microscopy)**

The Scanning Electron Microscope (SEM) is a microscope that uses electrons rather than light to form an image. There are many advantages to using the SEM instead of a light microscope.

The SEM has a large depth of field, which allows a large amount of the sample to be in focus at one time. The SEM also produces images of high resolution, which means that closely spaced features can be examined at a high magnification. Preparation of the samples is relatively easy since most SEMs only require the sample to be conductive. The combination of higher magnification, larger depth of focus, greater resolution, and ease of sample observation makes the SEM one of the most heavily used instruments in research areas today.

### **3.3. Magnetic and transport investigations**

#### **3.3.1. VSM (Vibrating Sample Magnetometer)**

Magnetic measurements were done in the temperature range 4.2 – 900 K using a VSM 12T Cryogen Free Magnet Cryogenic Ltd.

A vibrating sample magnetometer (VSM) operates on Faraday's Law of Induction, which tells us that a changing magnetic field will produce an electric field. This electric field can be measured and can give us information about the changing magnetic field. A VSM is used to measure the magnetic behavior of magnetic materials.

#### **3.3.2. Four-probe method**

The electrical resistivity was measured in a cryogen free magnet cryostat CFM - 7T (Cryogenic Ltd.) using the four-probe technique in the temperature range from 5 to 300 K and in magnetic fields up to 7T.

One of the most commonly used experimental technique is the co-linear four-probe (4-probe) method. This configuration consists of four independent electrical terminals where two terminals are used to apply current to the sample, and the other two terminals measure the resulting potential drop across a defined portion of the specimen.

#### **3.3.3. $\mu$ SR (Muon Spin Rotation/Relaxation/Resonance)**

$\mu$ SR (muon spin rotation) [25, 26-28] is a rather new experimental method. It offers, by its sensitivity to low magnetic moments (below  $10^{-3} \mu_B$ ) and the available time window (microseconds) information that cannot be obtained by other microscopic methods.  $\mu$ SR belongs to the family of NMR (Nuclear Magnetic Resonance), EPR (Electronic Paramagnetic Resonance), Neutron scattering and Mössbauer experimental methods. Applied to solid state physics, the  $\mu$ SR method is a very useful tool for the investigation of hyperfine fields, of the static and dynamic behavior of the nuclear and electronic magnetic moments, of critical phenomena etc. It is also sensitive to phase separation and therefore it is often used to distinguish between the competition and coexistence of different (magnetic) ground states.

## 4. Results

### 4.1. The $\text{Pr}_{1-x}\text{Sr}_x\text{CoO}_3$ system

#### 4.1.1. Sample preparation

High-quality  $\text{Pr}_{1-x}\text{Sr}_x\text{CoO}_3$  polycrystalline samples with  $x = 0.3, 0.4$  and  $0.5$  were prepared by standard ceramic reaction, using as raw materials high purity powders of  $\text{Pr}_6\text{O}_{11}$ ,  $\text{SrCO}_3$  and  $\text{Co}_3\text{O}_4$ .

#### 4.1.2. Structural analysis

Room temperature X-ray powder diffraction patterns were taken in a Bruker Advance D8 AXS Diffractometer using  $\text{Cu K}\alpha$  radiation. Rietveld refinements of the diffraction patterns were carried out using the TOPAS program. The X-ray diffraction patterns indicated that the samples were single perovskite phase, of orthorhombic ( $Pnma$ ) symmetry for  $x = 0.3$  and of monoclinic ( $P2_1/m$ ) symmetry for  $x = 0.4, 0.5$  with the unit cell parameters (Table 4.1) in close agreement with the values reported in earlier works.[29-32]

**Table 4.1.** Unit cell parameters for  $\text{Pr}_{1-x}\text{Sr}_x\text{CoO}_3$  system unit cell

x	Structure type	a(Å)	b(Å)	c(Å)	$\beta$
0.3	$Pnma$	5.42	7.60	5.37	90
0.4	$P2_1/m$	5.38	5.43	7.60	90.068
0.5	$P2_1/m$	5.38	5.41	7.62	90.255

The SEM pictures of the sintered powder  $\text{Pr}_{1-x}\text{Sr}_x\text{CoO}_3$  ( $x = 0.3, 0.4$  and  $0.5$ ) are shown in Figure 4.1. It can be seen that the particle size is about  $4 \mu\text{m}$ . There can also be observed in the same pictures, that the so called “inter-granular necks” which give a better conduction, are formed.

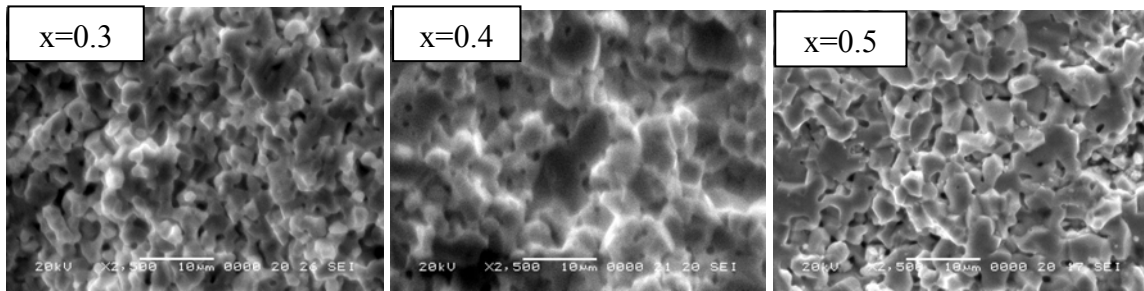


Figure 4.1. SEM images of  $\text{Pr}_{1-x}\text{Sr}_x\text{CoO}_3$  for  $x = 0.3, 0.4$  and  $0.5$  samples

Chemical analysis of the pellets obtained after pressing and sintering was carried out with an EDX spectrometer (Oxford Instruments) attached to a scanning electron microscope JSM 5600 LV type (JEOL company), located at the Technical University of Cluj-Napoca.

#### 4.1.3. Magnetic and transport properties of the $\text{Pr}_{1-x}\text{Sr}_x\text{CoO}_3$ compound

Magnetic investigations on  $\text{Pr}_{0.5}\text{Sr}_{0.5}\text{CoO}_3$  showed two phase transitions: a low temperature phase transition at  $T_A \approx 110$  K and a high temperature phase transition at  $T_C \approx 220$  K [30-32]. The high temperature transition at  $T_C$  is typical for cobaltites. The low temperature phase transition at  $T_A$  is still controversial. Mahendiran and Schiffer [30] found a maximum in coercivity around  $T_A$ ,

While the  $\text{PrCoO}_3$  is a paramagnetic insulator, the Sr-doped samples, with  $x = 0.3, 0.4$  and  $0.5$ , have a very different behavior. The temperature dependencies of resistivity for the samples  $\text{Pr}_{0.7}\text{Sr}_{0.3}\text{CoO}_3$  and  $\text{Pr}_{0.5}\text{Sr}_{0.5}\text{CoO}_3$  show a metallic behavior, in the high temperatures range and an intriguing upturn at low temperatures, below 100 K. In spite of the fact that this upturn is rather close to  $T_A$ , it seems to be not of intrinsic origin but probably arise from the carrier scattering processes at the grain boundaries from the polycrystalline samples, as seen in polycrystalline manganites and other transition metal oxides [35].

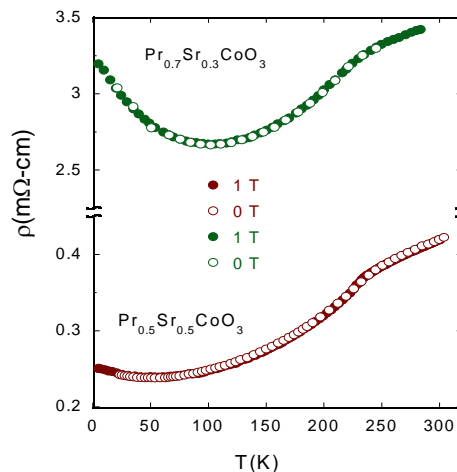
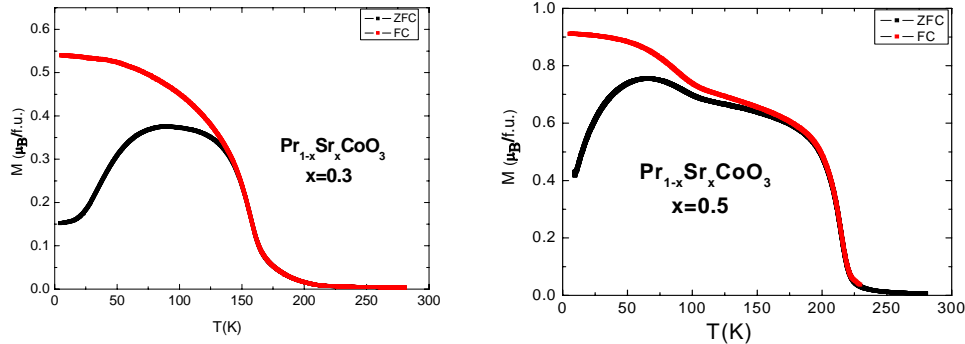


Figure 4.2. The temperature dependence of resistivity for  $x = 0.3$  and  $x = 0.5$ [36]

We found no sign of magnetic changes in the  $\rho(T)$  curves, at  $T_A$ . Probably, these changes are masked by disorder and grain boundary effects (Figure 4.2).



**Figure 4.3.** Magnetization after ZFC and FC for  $x = 0.3$  and  $x=0.5$  [36, 37]

Both FC and ZFC magnetization sharply increase below 240 K, at the Curie temperatures  $T_C$ 's in the case of the sample with  $x = 0.5$  and they show a feature below  $T_A$ 's, about 100 K. In the case of the sample with  $x = 0.3$  it can be seen that the temperature dependence of magnetization suggest ferromagnetic behavior with  $T_C \sim 160$  K.

ZFC magnetization curve in 0.1 T is different from the FC one suggesting a strongly increase of the magneto-crystalline anisotropy with decreasing temperature, below  $T_C$ . While the high temperature transition is similar [33] to other moderate-to-large bandwidth cobaltites, the second one is still controversial [34, 38] and it seems to be related with a change in the nature of magnetic interactions (Figure 4.3).

The transition temperatures were determinate as the minimum of  $\frac{\partial M}{\partial T}$  derivative.

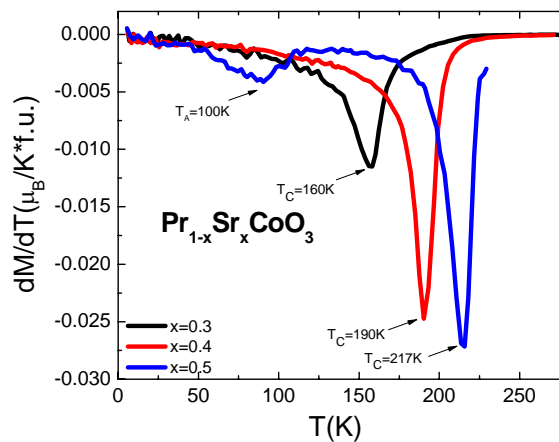


**Figure 4.4.** Determination of inflection point of the transition by using the numerical  $\partial M / \partial T$  derivative

Just like in the case of ZFC/FC measurements, the  $T_C$  transition temperatures can be observed at about 160K in the case of  $\text{Pr}_{0.7}\text{Sr}_{0.3}\text{CoO}_3$  and at about 190K in the case of the  $\text{Pr}_{0.6}\text{Sr}_{0.4}\text{CoO}_3$  sample, but no feature can be observed at lower temperatures. In the case of the  $\text{Pr}_{0.5}\text{Sr}_{0.5}\text{CoO}_3$  sample, both transition temperatures can easily be observed (Figure 4.4). The high temperature transition ( $T_C$ ) at about 220 K and a lower temperature transition ( $T_A$ ) at about 100 K.

The magnetization of the sample does not saturate even in 12 T, suggesting the existence of spin disorder in the system with  $\text{Co}^{3+}$  and  $\text{Co}^{4+}$  ions in different spin states and also the presence of coexisting paramagnetic and ferromagnetic states.

The signatures of the two magnetic transitions were also seen in ac susceptibility measurements (performed at 1000 Hz).  $\chi'(T)$  has a high and narrow peak corresponding to  $T_C$  and then it decreases with decreasing temperature and it has a small maximum in the region of  $T_A$ .

In order to investigate the MCE, the isothermal magnetization curves of the samples were measured with a field step of 1T in a range of 0–4T and a temperature step of 5 K over a range of temperatures around  $T_C$ .

To study the nature of the magnetic transition we built the Arrott plot and we used the Banerjee criterion [40]. In Figure 4.10 we plot the  $M^2$  versus  $M/H$  curves (Arrott plot) where a positive slope is clearly seen in all the  $M^2$  range, indicating that the phase transition is of second order (Figure 4.5).

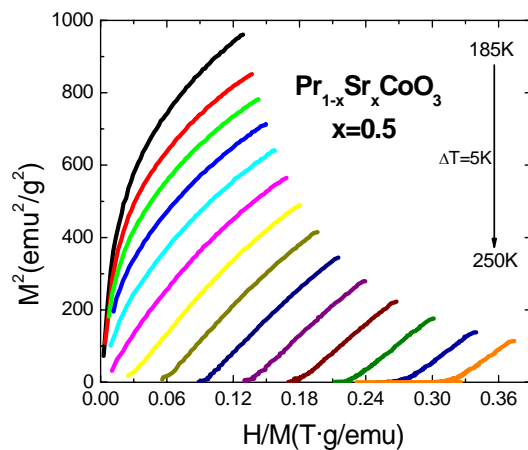


**Figure 4.5.** Arrott plot obtained from measured  $M$  vs.  $H$  isotherms, for the sample with  $x = 0.5$ .

The temperature dependences of magnetic entropy change in 1, 2, 3 and 4T external applied fields for the compound with  $x = 0.3$ , 0.4, and 0.5 are plotted in Figure 4.6 as example.

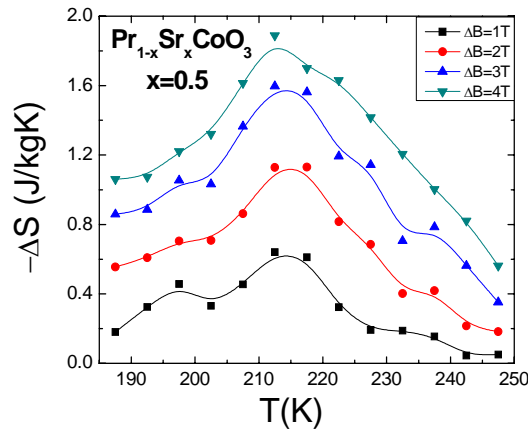


**Figure 4.6.** The temperature dependences of the magnetic entropy change for the samples with  $x = 0.5$ , in  $\Delta B = 1, 2, 3$  and  $4T$ .

The maximum values of entropy change occur almost around the transition temperatures for all the compounds.

The relative cooling power, RCP increases from the sample with  $x = 0.3$  to the sample with  $x=0.5$  as shown in the Table 4.2. Also from the table we can observe that the RCP values depend on the stoichiometry and they increase as the content of Pr decreases.

**Table 4.2.** The RCP values for the  $\text{Pr}_{0.7}\text{Sr}_{0.3}\text{CoO}_3$  and  $\text{Pr}_{0.6}\text{Sr}_{0.4}\text{CoO}_3$  and  $\text{Pr}_{0.5}\text{Sr}_{0.5}\text{CoO}_3$  samples

	RCP (J/Kg)		
	x=0.3	x=0.4	x=0.5
$\Delta B=4T$	56.73	70.84	107.14
$\Delta B=3T$	40.02	48.64	79.61
$\Delta B=2T$	23.03	29.14	45.97
$\Delta B=1T$	9.6	13.25	19.6

We have performed  $\mu$  SR experiments on  $\text{Pr}_{1-x}\text{Sr}_x\text{CoO}_3$  samples ( $x = 0.3, 0.4$  and  $0.5$ ). The results for all the samples are presented here in Figures 4.7, 4.8.

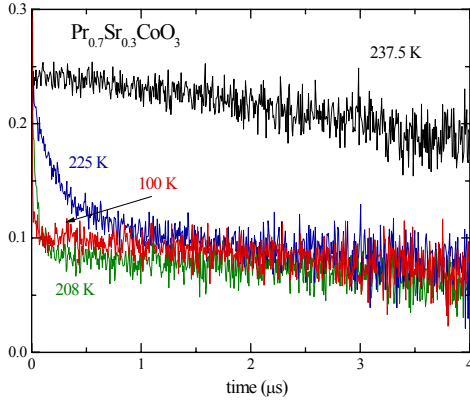


**Figure 4.7.**  $\mu$ SR spectra recorded at temperatures around the magnetic phase transition rate for the sample  $\text{Pr}_{0.7}\text{Sr}_{0.3}\text{CoO}_3$ . [36, 39]

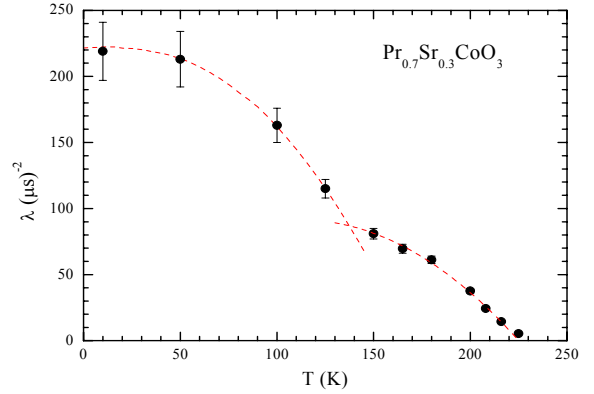


**Figure 4.8.** Temperature dependence of relaxation rate for the sample  $\text{Pr}_{0.7}\text{Sr}_{0.3}\text{CoO}_3$  [36, 39]

As shown in, Figure 4.8,  $\lambda(T)$  clearly indicates a double magnetic transition. It follows the temperature dependence of the order parameter. From these data we can only infer that since the high temperature ferromagnetic transition at  $T_C$  is induced by doping, the low temperature transition at  $T_A$  results from a change in the nature of magnetic coupling between Co ions. [39]

#### 4.1.4. Preliminary Conclutions

Polycrystalline samples  $\text{Pr}_{1-x}\text{Sr}_x\text{CoO}_3$  ( $x = 0.3, 0.4$  and  $0.5$ ) were investigated by conventional magnetic measurements, as well as by  $\mu$ SR method.

A double magnetic transition was found in  $\text{Pr}_{1-x}\text{Sr}_x\text{CoO}_3$  ( $x = 0.3, 0.4$  and  $0.5$ ) by using magnetic and  $\mu$ SR measurements. The high-temperature transition is typical for Sr-doped cobaltites, while the other transition occurs as a result of the change in the nature of the magnetic interactions between the Co ions.

The electrical measurements indicate low magnetoresistance, metallic behavior at high temperatures and grain boundary scattering effect in the low temperatures region.

## 4.2. The $\text{Pr}_{0.7}(\text{Ca}_{1-x}\text{Sr}_x)_{0.3}\text{CoO}_3$ system

### 4.2.1. Sample preparation

The  $\text{Pr}_{0.7}(\text{Ca}_{1-x}\text{Sr}_x)_{0.3}\text{CoO}_3$  compounds with  $x = 0, 0.2, 0.5, 0.7, 0.8$  si  $0.95$ , were prepared by conventional solid-state reaction.

### 4.2.2. Structural analysis

The powder X-ray diffraction patterns were recorded by using a Bruker D8 Advance AXS diffractometer with  $\text{Cu K}_\alpha$  radiation. The data were refined by the Rietveld method using the program TOPAS. All the samples are single phase without detectable secondary phase, within the sensitivity limits of the experiment, and they have orthorhombic  $\text{Pnma}$  type structure.

### 4.2.3. Magnetic and transport properties of the $\text{Pr}_{0.7}(\text{Ca}_{1-x}\text{Sr}_x)\text{CoO}_3$ compound

The resistivity for all the samples were measured in another cryogen free magnet cryostat CFM-7 T (Cryogenic Ltd.) by the four-probe technique, in the temperature range from 5 to 300K and magnetic fields up to 7 T.

The samples have semiconducting behavior at low temperatures, in spite of their very low values of the electrical resistivity.

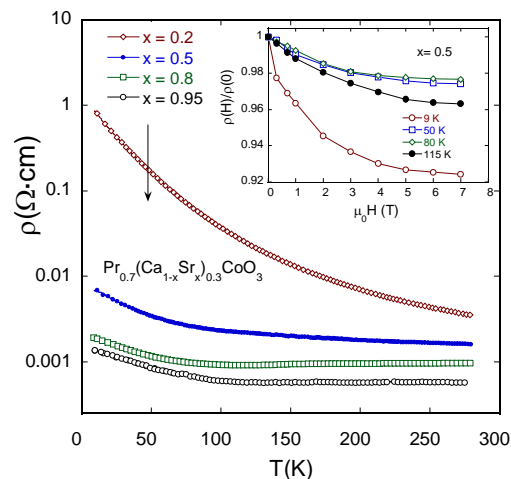


**Figure 4.9.** The temperature dependence of electrical resistivity in zero applied magnetic field, for the samples with  $x = 0.2, 0.5, 0.8$  and  $0.95$ . In inset:  $\rho(H)/\rho(0)$  measured at 9 K, 50 K, 80 K and 150 K for the sample with  $x = 0.95$ . [43]

The samples with  $x > 0.5$  have metallic behavior down to about 100 K, and then they have semiconductor behavior ( $dp/dT < 0$ ) at lower temperatures, probably, due to grain boundary effects [42].

All the samples showed negative magnetoresistance. For the samples with high Ca content the magnetoresistance is maximum at the lowest temperature and in 7T, as can be seen in the inset of Figure 4.9 (inset).

The cobaltite  $\text{Pr}_{0.7}\text{Ca}_{0.3}\text{CoO}_3$ , shows also the features of glassy behavior, indicating an inhomogeneous magnetic system. The temperature dependence of magnetization has history dependence with a bifurcation between ZFC and FC curves at an irreversibility temperature  $T_{\text{irr}}$ , as illustrated in Figure 4.10.

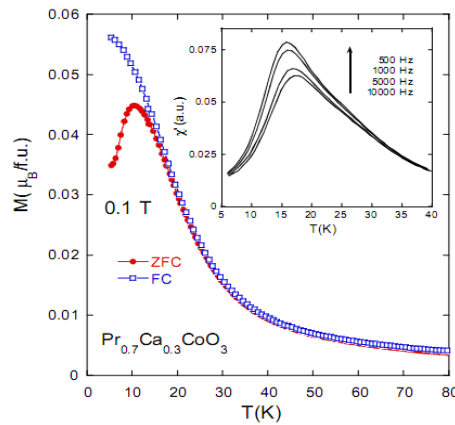


**Figure 4.10.** Field cooled and zero field cooled magnetizations of  $\text{Pr}_{0.7}\text{Ca}_{0.3}\text{CoO}_3$  as a function of temperature. In the inset,  $\chi'(T)$  is plotted at selected frequencies [44].

The ac susceptibility is frequency dependent showing sharp maxima, both in the real part  $\chi'(T)$  and in the imaginary part  $\chi''(T)$ . In the inset of Figure 4.24,  $\chi'(T)$  is plotted at selected frequencies. Here again, the temperature  $T_{\text{r}} \sim 16$  K corresponding to the peak was found to be linear in the logarithm of the frequency.

The rapid increase of  $M$  around  $T_{\text{C}}$  signals the phase transition from a paramagnetic to an ordered state, as shown in Figure 4.11 for the samples with  $x = 0.5$  and  $0.95$ . The temperature dependence of magnetization is strongly dependent on magnetic history starting from a temperature just below  $T_{\text{C}}$  to the lowest temperature with a bifurcation between ZFC and FC data at an irreversibility temperature  $T_{\text{irr}}$ .

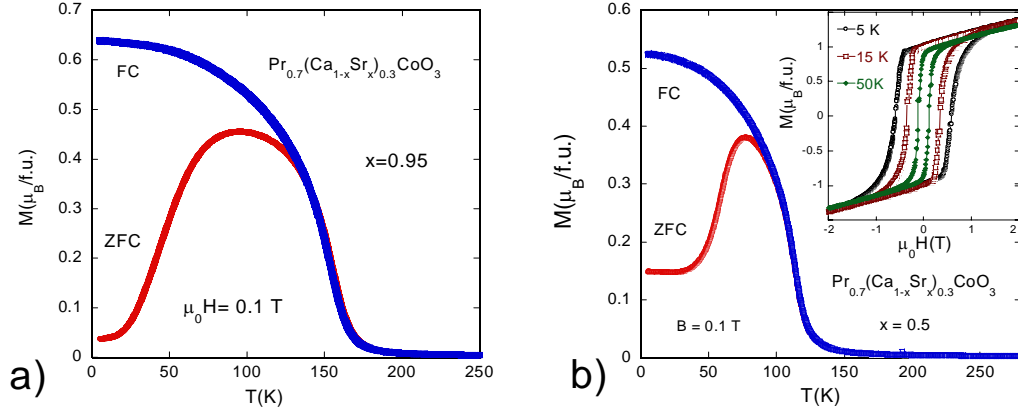


**Figure 4.11.** Field cooled (FC) and zero field cooled (ZFC) magnetization of  $\text{Pr}_{0.7}(\text{Ca}_{1-x}\text{Sr}_x)_{0.3}\text{CoO}_3$  as a function of temperature, measured in 0.1 T. For a)  $x = 0.95$ , b)  $x = 0.5$ , (in inset: the hysteresis loops at 5, 15 and 50K).[43]

The bifurcation between  $M_{\text{ZFC}}(T)$  and  $M_{\text{FC}}(T)$  curves is typical for doped cobaltites [45, 46].

The hysteresis loops indicate that all the samples have ferromagnetic like behavior, as shown in inset of Figure 4.11 b) for the sample with  $x = 0.5$ .

We also calculated the transition temperatures as the minimum of the  $\frac{\partial M}{\partial T}$  derivative.

It was observed that the values of the  $T_C$ 's of our samples increase as the content of Ca decreases.(Figure 4.12)

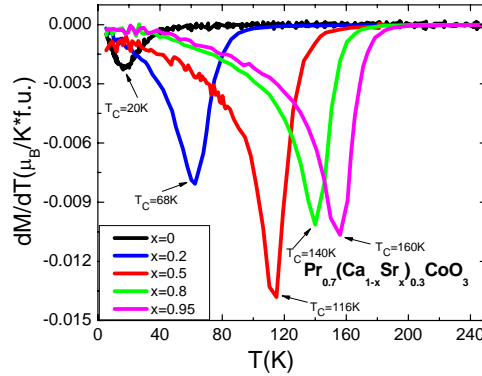


**Figure 4.12.** Determination of inflection point of the transition by using the numerical  $\partial M/\partial T$  derivative

No saturation was seen in  $M(H)$  curves for any of the samples, even up to 9 T.

Such a behavior suggests the coexistence of a dominant ferromagnetic phase together with a non-ferromagnetic one, i.e., a phase separation scenario.

To study the nature of the magnetic transition we built the Arrott (Figure4.13) plot and we used the Banerjee criterion [40]. The second-order magnetic transition, present here,

at  $T_C$  induces a smaller MCE but with a distribution over a broader temperature range, thus resulting in a larger RCP.

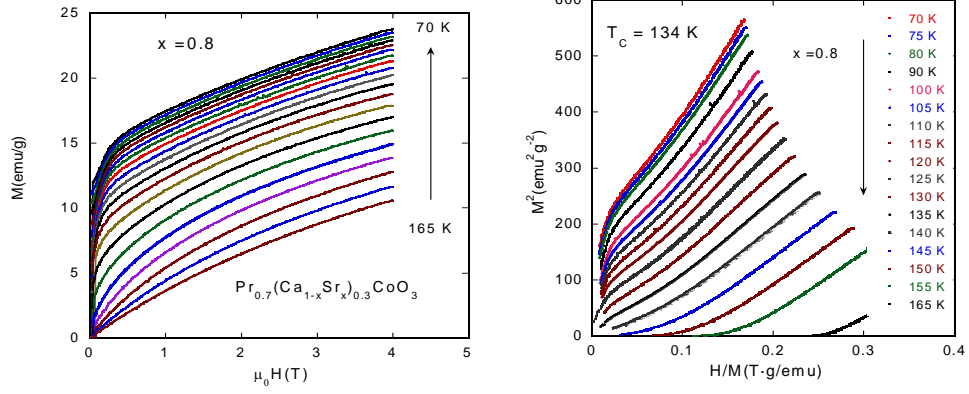


**Figure 4.13.** Isothermal magnetization curves taken at different fixed temperatures between 70 and 165K for the  $\text{Pr}_{0.7}(\text{Ca}_{0.2}\text{Sr}_{0.8})_{0.3}\text{CoO}_3$  cobaltite. (b) Arrot plot obtained from measured  $M$  vs.  $H$  isotherms, for the sample with  $x = 0.8$  [43].

The temperature dependences of magnetic entropy change in 1, 2, 3 and 4T external applied fields for the compound with  $x = 0.2$ , and 0.95 are plotted in Figure 4.14, as examples. The maximum values of entropy change occur almost around the transition temperatures for all the compounds.

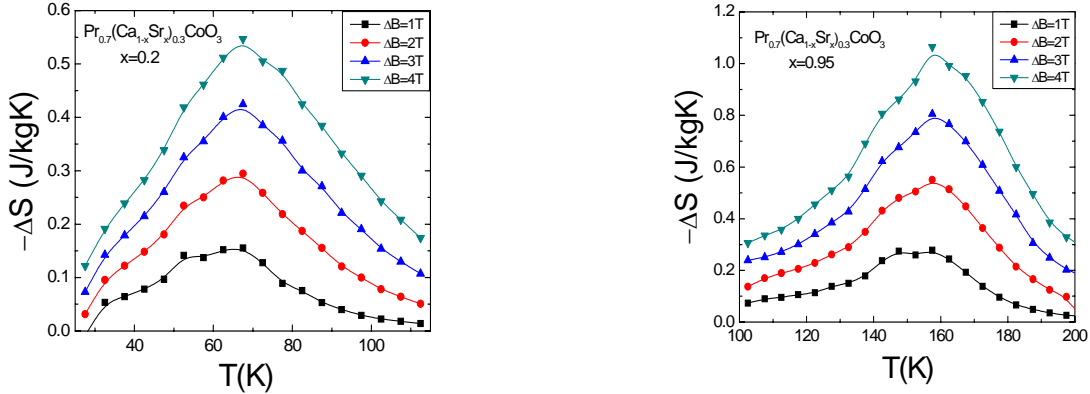


**Figure 4.14.** The temperature dependences of the magnetic entropy change for the samples with  $x = 0.2$ , and  $x=0.95$  in  $\Delta B = 1, 2, 3$  and  $4$  T [43].

We cannot talk about a significant MCE for the sample with  $x = 0$  since, we have a low magnitude of magnetization and a broaden transition, with a distribution of  $T_C$ 's that lead to negligible values for  $(\partial M(T, H) / \partial T)_H$ .

By using these (Ca, Sr) doping, with  $x > 0.2$ , the values of the relative cooling powers will not change very much, but they could be used in different temperature ranges. The

values for RCP are somewhat smaller than those obtained in doped manganite perovskites but they are high enough for technical interest. (values shown in Table4.3)

**Table 4.3.** The RCP values for the  $\text{Pr}_{0.7}(\text{Ca}_{1-x}\text{Sr}_x)\text{CoO}_3$  ( $x=0.2, 0.5, 0.8$  and  $0.95$ ) samples

	<b>RCP (J/Kg)</b>			
	<b>x = 0.2</b>	<b>x = 0.5</b>	<b>x = 0.8</b>	<b>x = 0.95</b>
<b><math>\Delta B = 4\text{T}</math></b>	31.46	53.5	54.9	59.85
<b><math>\Delta B = 3\text{T}</math></b>	22.03	41.6	44.8	42.86
<b><math>\Delta B = 2\text{T}</math></b>	13.57	29.4	30.2	26.64
<b><math>\Delta B = 1\text{T}</math></b>	6.23	15.2	15.7	12.07

#### 4.2.4. Preliminary Conclusions

High-quality samples of  $\text{Pr}_{0.7}(\text{Ca}_{1-x}\text{Sr}_x)_{0.3}\text{CoO}_3$  ( $x = 0, 0.2, 0.5, 0.8, 0.95$ , and  $1$ ) were prepared by standard ceramic reaction, and their magnetic and electrical properties were investigated. All the compounds crystallize in an orthorhombic structure.  $\text{Pr}_{0.7}\text{Ca}_{0.3}\text{CoO}_3$  has cluster-glass behavior, with no long range magnetic order. When Sr partially replaces Ca in this system, the cluster-glass behavior is suppressed and the magnetism is enhanced. Similarly, the electrical conduction is improved with increasing Sr content in the samples.

All the samples have negative magnetoresistance at low temperatures. The electrical conduction is percolative and controlled by grain boundary effects.

### 4.3. The $\text{Nd}_{1-x}\text{Sr}_x\text{CoO}_3$ system

#### 4.3.1. Sample preparation

Ceramic samples with nominal composition  $\text{Nd}_{1-x}\text{Sr}_x\text{CoO}_3$  ( $x = 0.3$  and  $0.5$ ) were synthesized using the conventional solid state reaction method.

#### 4.3.2. Structural analysis

The X-ray powder diffraction (XRPD) patterns were recorded at room temperature using a Bruker Advance D8 AXS diffractometer with  $\text{CuK}_\alpha$  radiation. The data were refined by the Rietveld method using the program TOPAS.

For the  $\text{Nd}_{1-x}\text{Sr}_x\text{CoO}_3$  samples ( $x = 0.3$  and  $0.5$ ), X-ray diffraction data indicated the samples are single-phase with the expected orthorhombic structure and lattice parameters (Table 4.4) in close agreement with the values reported in earlier works.

**Table 4.4.** Unit cell parameters for  $\text{Nd}_{1-x}\text{Sr}_x\text{CoO}_3$  system unit

<b>x</b>	<b>0.3</b>	<b>0.5</b>
<b>a[Å]</b>	<b>5.36</b>	<b>5.37</b>
<b>b[Å]</b>	<b>5.40</b>	<b>5.41</b>
<b>c[Å]</b>	<b>7.59</b>	<b>7.61</b>
<b>V[Å<sup>3</sup>]</b>	<b>220.41</b>	<b>221.78</b>
<b>Cry Size (nm)</b>	<b>69.06</b>	<b>57.09</b>
<b>R<sub>Bragg</sub></b>	<b>1.53</b>	<b>1.82</b>

### 4.3.3. Magnetic properties and transport properties

The results of our magnetic measurements (magnetization and ac susceptibility) on polycrystalline  $\text{Nd}_{0.7}\text{Sr}_{0.3}\text{CoO}_3$  and  $\text{Nd}_{0.5}\text{Sr}_{0.5}\text{CoO}_3$  samples are similar to those already reported [47, 48]  $T_C \sim 140$  K and  $T_F \sim 40$  K for the  $\text{Nd}_{0.7}\text{Sr}_{0.3}\text{CoO}_3$  sample while  $T_C \sim 200$  K and  $T_F \sim 45$  K for the  $\text{Nd}_{0.5}\text{Sr}_{0.5}\text{CoO}_3$  sample.

From the  $M^2$  versus  $M/H$  curves (Arrott plot) where a positive slope is clearly seen in all the  $M^2$  range, indicating that the phase transition is of second order we were able to determine the transition temperature for the sample with  $x=0.3$  being of about 140K.

The  $\mu\text{SR}$  experiments also revealed the unusual magnetic properties of these compounds. Examples  $\mu\text{SR}$  spectra recorded at selected temperatures for  $\text{Nd}_{0.5}\text{Sr}_{0.5}\text{CoO}_3$  are displayed in Figure 4.15. The solid lines in Figure 4.15 represent the best fits to the data of the above equation for  $AP(t)$ .

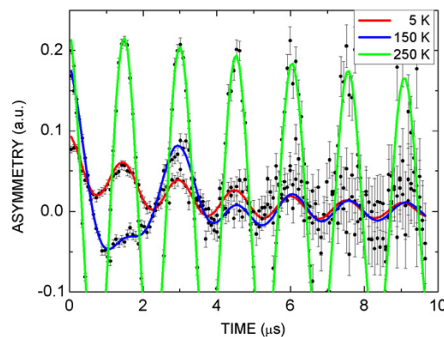


**Figure 4.15.**  $\mu\text{SR}$  spectra for  $\text{Nd}_{0.5}\text{Sr}_{0.5}\text{CoO}_3$  recorded in wTF mode at selected temperatures: 5, 150 and 250K[41].

$A_{para}(T)$  for  $Nd_{0.5}Sr_{0.5}CoO_3$  is plotted in Figure 4.16. It drops towards zero with decreasing temperature, between 200 and 125 K, indicating a large magnetic phase transition, from the paramagnetic to the ferromagnetic state observed in the bulk magnetization measurements.

The temperature dependence of the 1/3 term's relaxation rate  $\lambda_m$  and of the paramagnetic asymmetry  $A_{para}$  are plotted in Figure 4.16, together with the temperature dependencies of the FC and ZFC magnetization,  $M(T)$ , solid lines. Contrary to the results obtained for the Pr compounds, the magnetic ordering is not static in  $Nd_{1-x}Sr_xCoO_3$ : the relaxation rate of the 1/3 term  $\lambda_m$ , is not zero below  $T_C$  ( $\lambda_m = 0.29 \mu s^{-1}$  at 29 K), see Figure 4.16. It even increases below about 45 K mimicking the approach to another phase transition.

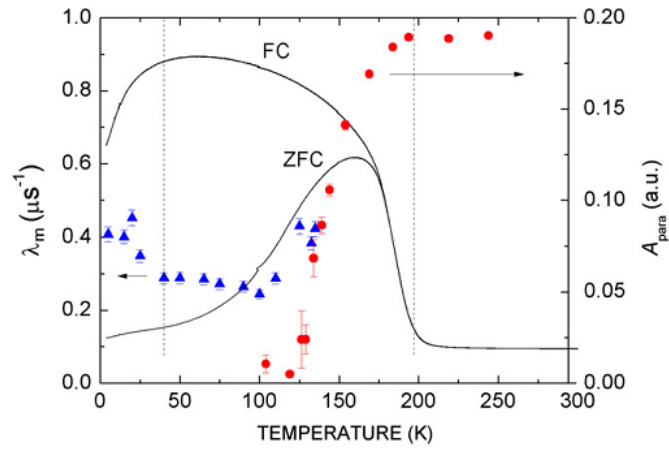


**Figure 4.16.**  $A_{para}(T)$  and  $m(T)$  for  $Nd_{0.5}Sr_{0.5}CoO_3$ . Solid line: the temperature dependence of the FC and the ZFC magnetization.[41]

#### 4.3.4. Preliminary conclusions

Our magnetic measurements results on  $Nd_{0.7}Sr_{0.3}CoO_3$  and  $Nd_{0.5}Sr_{0.5}CoO_3$  samples are in excellent agreement to previously reported studies in literature.

The onset of the induced ferromagnetic order of the Nd sublattice in the  $Nd_{1-x}Sr_xCoO_3$  compounds is marked by an increase of the muon spin depolarization rate  $\lambda_m(T)$  below  $\sim 45$  K. Our  $\mu$ SR data do not show evidence of phase separation in these two systems.

#### 4.4. The $\text{La}_{1.2}\text{R}_{0.2}\text{Ca}_{1.6}\text{Mn}_2\text{O}_7$ compounds (with R = Nd, Ho, Yb)

##### 4.4.1. Sample preparation

Polycrystalline samples with nominal composition  $\text{La}_{1.2}\text{R}_{0.2}\text{Ca}_{1.6}\text{Mn}_2\text{O}_7$  compounds where R = La, Nd, Ho or Yb were prepared by standard ceramic reaction from high purity materials (oxides and carbonates) at high temperatures.

##### 4.4.2. Structural analysis

The powder X-ray diffraction patterns were recorded by using a Bruker D8 Advance AXS diffractometer with Cu  $K\alpha$  radiation. The X-ray diffraction patterns for all the prepared samples showed mainly clean single phase compounds (Figure 4.17).

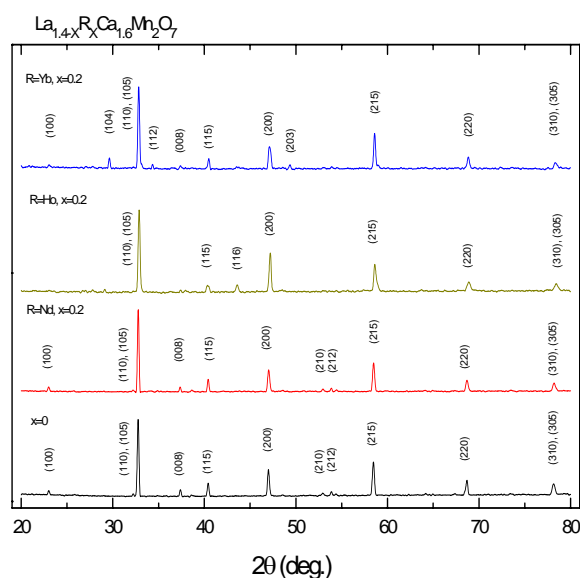
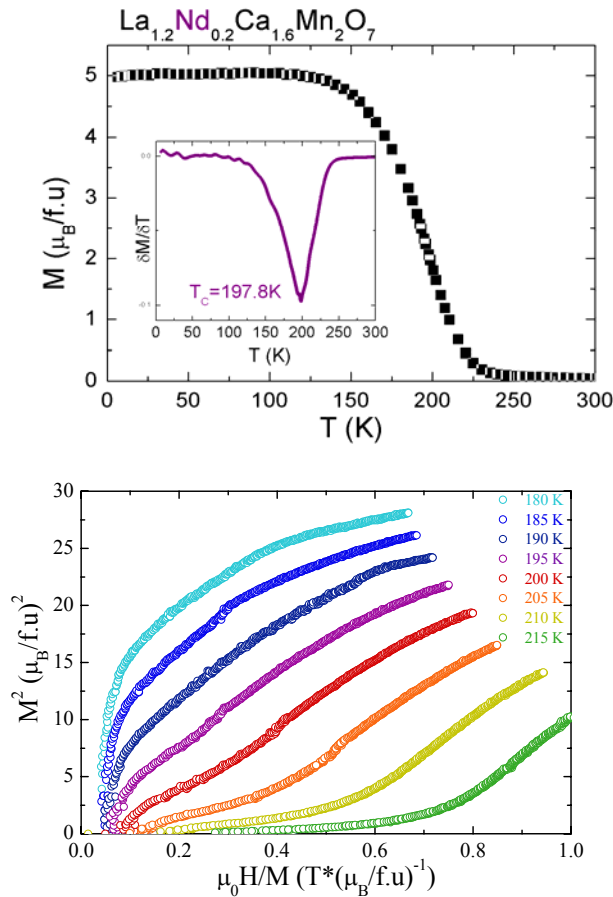


Figure.4.17. Diffraction patterns for  $\text{La}_{1.4-x}\text{R}_x\text{Ca}_{1.6}\text{Mn}_2\text{O}_7$  compounds.[49]

##### 4.4.3. Magnetic measurements

The magnetization measurements do not show saturation for the studied samples. One can see that a transition from a ferromagnetic order to a paramagnetic one is present. The Curie temperatures were determined from Arrott plots and from the temperature dependences of the magnetization, in low field ( $B=0.03$  T), at temperatures where  $dM/dT$  have minima.



**Figure. 4.18.** (up) the temperature dependence of the magnetization in a 0.03 T magnetic field with an inset containing the temperature dependence of  $dM/dT$ ; (down) Arrot plot for  $\text{La}_{1.2}\text{Nd}_{0.2}\text{Ca}_{1.6}\text{Mn}_2\text{O}_7$  [49]

The Curie temperatures decrease when La is substituted by rare earths ions. The diminution of the Curie temperatures can be correlated with the structural changes. The  $\text{R}^{3+}$  radius are smaller as compared with  $\text{La}^{3+}$  one and induced a stronger structural distortion which has as result a tilting of the Mn-O-Mn angle and a diminution of the exchange interactions. The anomalous magnetization plateau above the Curie temperature can be explained by the presence of a two dimensional (2D) short range magnetic order.

At temperatures below 400 K the temperature dependence of the reciprocal susceptibility is not linear, probable due to appearance of clusters.

The ZFC and FC curves show differences at low temperatures, indicating a spin-glass-like behavior.

The anisotropic spin glass state appears due to frustration of random competing double/exchange ferromagnetic and super-exchange antiferromagnetic interactions together with the anisotropy originating from layered structure. The competition of antiferromagnetic

and ferromagnetic interactions can lead to the frustration, which is responsible for spin glass-like (cluster glass) behavior observed in some perovskite manganites and cobaltites.

The maximum values of  $|\Delta S|$  are at temperatures very close to the magnetic transition ones. One can see that the curves are almost symmetrical at two sides of their peak value. In general this phenomenon is characteristic of a second order magnetic transition [50].

Another advantage of these materials for the magnetic refrigeration is the broadening of the magnetic entropy peaks and the easy way to tune the transition temperature.

#### **4.4.4. Preliminary Conclusions**

The structure, magnetic properties and the magnetic entropy change of  $\text{La}_{1.4-x}\text{R}_x\text{Ca}_{1.6}\text{Mn}_2\text{O}_7$  compounds where  $\text{R} = \text{Nd}, \text{Sm}, \text{Ho}$  or  $\text{Yb}$  have been investigated. The substitution of R atoms for La does not affect the crystal structure but it leads to a small decrease of the lattice parameters. The Curie temperatures decrease when La is substituted by R atoms.

The anomalous magnetization plateau above the Curie temperature can be explained by the presence of a two dimensional (2D) short range magnetic order.

The anisotropic spin glass state confirmed by ZFC and FC measurements appears due to frustration of random competing double exchange ferromagnetic and super-exchange antiferromagnetic interactions together with the anisotropy originating from layered structure.

The maximum values of the magnetic entropy change are at temperatures very close to the magnetic transition ones.

The RCP(S) values together with the broadening of the magnetic entropy peaks and the possibility to tune the transition temperature show the advantages of these materials for the magnetic refrigeration.

## **Conclusions**

The structural, electronic and magnetic properties of  $\text{Pr}_{1-x}\text{Sr}_x\text{CoO}_3$ ,  $\text{Pr}_{0.7}(\text{Ca}_{1-x}\text{Sr}_x)_{0.3}\text{CoO}_3$ ,  $\text{Nd}_{1-x}\text{Sr}_x\text{CoO}_3$  and  $\text{La}_{1.2}\text{R}_{0.2}\text{Ca}_{1.6}\text{Mn}_2\text{O}_7$  compounds were investigated by X-ray diffraction, magnetization and magnetic susceptibility measurements, Scanning Electron Microscopy and Muon Spin Rotation/Relaxation/Resonance. The performed substitutions had

significant changing effects in the structural electronic and magnetic properties of all of the compounds.

The conclusions regarding the studied compounds are as follows:

- $\text{Pr}_{1-x}\text{Sr}_x\text{CoO}_3$  ( $x=0.3, 0.4, \text{ and } 0.5$ ),  $\text{Pr}_{0.7}(\text{Ca}_{1-x}\text{Sr}_x)_{0.3}\text{CoO}_3$  ( $x = 0, 0.2, 0.5, 0.7, 0.8, 0.95, \text{ and } 1$ ),  $\text{Nd}_{1-x}\text{Sr}_x\text{CoO}_3$  ( $x=0.4 \text{ and } 0.5$ ) and  $\text{La}_{1.2}\text{R}_{0.2}\text{Ca}_{1.6}\text{Mn}_2\text{O}_7$  ( $\text{R}=\text{La, Nd, Ho, Yb}$ ) were all prepared by standard ceramic reaction from high purity materials (oxides and carbonates) at high temperatures.
- X-ray diffraction showed single phase for all the compounds.
- For the  $\text{Pr}_{1-x}\text{Sr}_x\text{CoO}_3$ ,  $\text{Pr}_{0.7}(\text{Ca}_{1-x}\text{Sr}_x)_{0.3}\text{CoO}_3$ ,  $\text{Nd}_{1-x}\text{Sr}_x\text{CoO}_3$  compounds an increase in the values of the Currie temperature can be observed along with the increase of the Sr doping. In the case of the  $\text{La}_{1.2}\text{R}_{0.2}\text{Ca}_{1.6}\text{Mn}_2\text{O}_7$  compound it was recorded a decrease in the values of the Currie temperature as the substitution of La atoms with R (Ho, Yb, Nd) atoms takes place.
- A double magnetic transition was found in  $\text{Pr}_{1-x}\text{Sr}_x\text{CoO}_3$  ( $x = 0.3, 0.4 \text{ and } 0.5$ ). The high-temperature transition is typical for Sr-doped cobaltites, while the other transition occurs as a result of the change in the nature of the magnetic interactions between the Co ions. The two transitions are confirmed by the  $\mu\text{SR}$  measurements. The magnetic entropy variation reaches the highest values in the case of the sample with  $x=0.5$  and also cover a large range of temperature of about 60 degrees.
- In the case of  $\text{Pr}_{0.7}(\text{Ca}_{1-x}\text{Sr}_x)_{0.3}\text{CoO}_3$  system for the samples with  $x > 0$  a ferromagnetic-like behavior is observed (ferromagnetic order but with a possible coexistence of superparamagnetic clusters) below the transition temperature.  $\text{Pr}_{0.7}\text{Ca}_{0.3}\text{CoO}_3$  has cluster-glass behavior, with no long range magnetic order but as the Sr partially replaces Ca in this system, the cluster-glass behavior is suppressed, the magnetism is enhanced and the electrical conduction is improved. All the samples have negative magnetoresistance at low temperatures. By (Ca, Sr) doping in this system we can obtain rather high cooling powers in various temperature ranges, with reasonably good magnetocaloric values.
- Our magnetic measurements (magnetization and ac susceptibility) results on  $\text{Nd}_{0.7}\text{Sr}_{0.3}\text{CoO}_3$  and  $\text{Nd}_{0.5}\text{Sr}_{0.5}\text{CoO}_3$  samples are in excellent agreement to previously reported studies in literature

The onset of the induced ferromagnetic order of the Nd sublattice (coupled antiparallel to the Co lattice) in the  $\text{Nd}_{1-x}\text{Sr}_x\text{CoO}_3$  compounds is marked by an increase of the muon spin depolarization rate  $\lambda_m(T)$  below  $\sim 45$  K. Our  $\mu\text{SR}$  data do not show evidence of phase separation in these two systems.

- The anomalous magnetization plateau above the Curie temperature, in the case of  $\text{La}_{1.2}\text{R}_{0.2}\text{Ca}_{1.6}\text{Mn}_2\text{O}_7$  can be explained by the presence of a two dimensional (2D) short range magnetic order. The anisotropic spin glass state confirmed by ZFC and FC measurements appears due to frustration of random competing double exchange ferromagnetic and super-exchange antiferromagnetic interactions together with the anisotropy originating from layered structure. The maximum values of the magnetic entropy change are at temperatures very close to the magnetic transition ones. The magnetic entropy curves are characteristic of a second order magnetic transition and their decrease in the maximum values with composition can be attributed to the diminution of the exchange interactions due to substitutions.

## Selected References

- [1] M. A. Señaris-Rodríguez and J. B. Goodenough, *J. Solid State Chem.* **118**, (1995) 323.
- [2] R. Von Helmolt, J. Wecker, B. Holzapfel, L. Schultz, K Samwer, *Phys. Rev. Lett.* 71 (1993) 2331.
- [3] G. Radaelli, D.E. Cox, M. Marezio, S.-W. Cheong, P.E Schiffer, A.P. Ramirez, *Phys. [4]Rev. Lett.* 75 (1995) 4488.
- [5] A. Maignan, C. Martin, D. Pelloquin, N. Nguyen, and B. Raveau, *J. Solid State Chem.* 142, 247 (1999).
- [6] K.-I. Kobayashi, T. Kimura, H. Sawada, K. Terakura, and Y. Tokura, *Nature (London)* 395, 677 (1998).
- [7] J. Nakamura, J. Lindén, T. Yamamoto, M. Karppinen, H. Yamauchi, and T. Pietari, *Appl. Phys. Lett.* 76, 2925 (2000).
- [8] Y. Moritomo, A. Asamitsu, H. Kuwahara, Y. Tokura, *Nature* 380 (1996) 141.
- [9] J.B. Philipp, J. Klein, C. Recher, T. Walther, W. Mader, M. Schmid, R. Suryanarayanan, L. Alff, R. Gross, *Phys. Rev. B* 65 (2002) 184411.
- [10] *Advances in Physics*, 1999, Vol. 48, No. 2, 167- 293
- [11] Mark R. Levy, PhD Thesis, Department of Materials imperial College of Science, Technology and Medicine January 2005
- [12] *Journal of Magnetism and Magnetic Materials* 200 (1999) 1-23
- [13] C. Zener. *Phys. Rev.*, 81:440, 1951.
- [14] H. A. Kramers. *Physica*, 1:182, 1934.
- [15] P. W. Anderson. *Phys. Rev.*, 79:350, 1950.
- [16] P. W. Anderson. *Phys. Rev.*, 80:922, 1950.
- [17] Pecharsky V.K., Gschneider K.A. Jr., *J. Magn. Magn. Mater.*, 200 (1999), 44.
- [18] Tishn A.M., [in:] *Handbook of Magnetic Materials*, K.H.J. Buschow (Ed.), Elsevier, Amsterdam, 1999, vol.12, p. 395
- [19] Gschneider K.A. Jr., Pecharsky V.K., Pecharsky A.O., Zimm C.B., *Rare Earth' 98*, 315-3 (1999), 69.
- [20] P. A Cox. *Transition Metal Oxides*. Oxford, Clarendon, 1992.
- [21] Coldea Marin, *Magnetorezistenta. Efecte si aplicatii*. Editura Presa Universitara Clujana, 2009
- [22] V. Pop, I. Chicinas, N. Jumate, *Fizica Materialelor.Metode Experimentale*, Editura Presa Universitara Clujana, 2001
- [23] *Structure, Properties and Preparation of Perovskite-type Compounds*, R.Smolunhowski and N. Kurti
- [24] C. J. Brinker and G. W. Sherer, "Sol-Gel Science", Academic Press, San Diego, 1990.
- [25] A. Amato, D. Andreica, *Muon Spin Rotation*, in *Encyclopedia of Condensed Matter*, eds. F. Bassani, G. Liedl, P. Wider, Elsevier, 2005
- [26] G.M. Kalvius et al., In: Gschneider KA (eds.) *Handbook on the Physics and Chemistry of Rare Earths*, vol. 32, p. 55. Amsterdam: North-Holland, (2001).
- [27] P. Dalmas de Reotier and A. Yaouanc, *Journal of Physics: Condensed Matter* 9 (1997) 9113.
- [28] A. Schenck *Muon Spin Rotation Spectroscopy*. Bristol:Adam Hilger, (1985).
- [29] H.W. Brinks, H. Fjellvag, A. Kjekshus, B.C. Hauback, *J. Solid State Chem.* 147 (1999) 464.
- [30] R. Mahendiran, P. Schiffer, *Phys. Rev. B* 68 (2003) 024427.
- [31] I.O. Troyanchuk, D.V. Karpinski, A.N. Chobot, D.G. Votsekhovich, V.M. Dobryanski, *JETP Lett.* 84 (2006) 151.
- [32] S. Hirahara, Y. Nakai, K. Miyoshi, K. Fujiwara, J. Takeuchi, *J. Magn. Magn. Mater.* 310 (2007) 1866.
- [33] J.-Q. Yan, J.-S. Zhou, J.B. Goodenough, *Phys. Rev. B* 69 (2004) 134409.
- [34] M. Uchida, R. Mahendiran, Y. Tomioka, Y. Matsui, K. Ishizuka, Y. Tokura, *Appl. Phys. Lett.* 86 (2005) 131913.
- [35] M. Ziese, *Rep. Prog. Phys.* 65 (2002) 143.
- [36] I. G. Deac, R. Tetean, I. Balasz, D. Andreica, **A. Vlădescu**, R. Dudric, A. R. Tunyagi, E. Burzo; *Journal of Physics: Conference Series* 200 (2010) 052003
- [37] I. G. Deac, **A. Vlădescu**, I. Balasz, A. Tunyagi and R. Tetean; *International Journal of Modern Physics B* Vol. 24, Nos. 6 & 7 (2010) 762–769
- [38] L. Wang, N. A. Frey, H. Srikanth, J. E. Davies, Kai Liu, and J. F. Mitchell, *Phys.Rev. B* 79, 214420 (2009).
- [39] I.G. Deac , D. Andreica, I. Balasz, **A. Vladescu**, Roxana Dudric, R. Tetean; *Physica B* 406 (2011) 2795–2800
- [40] S.K. Banerjee, *Phys. Lett.* 12, 16 (1964).
- [41] I.G. Deac, R.Tetean, D. Andreica, E.Burzo, *IEEE Trans. Magn.* **44**, (2008) 2922.
- [42] M. Ziese, *Rep. Prog. Phys.* 65,143 (2002).

- [43] I.G. Deac, **A. Vlădescu**, I. Balasz, A. Tunyagi and R. Tetean, Acta Physica Polonica A, Vol. 120 (2011)  
[44] I. G. Deac, **A. V. Vlădescu**, Studia Universitatis BABES-BOLYAI, PHYSICA, LV, 1, 2010  
[45] V.K. Sharma, M.K. Chattopadhyay, S.B. Roy, J. Phys. D: Appl. Phys. 40, 1869 (2007).  
[46] H.M. Aarbhogh, J. Wu, L. Wang, H. Zheng, J.F. Mitchell, C. Leighton, Phys. Rev. B 74, 134408 (2006).  
[47] A. Ghoshray, B. Bandyopadhyay, K. Ghoshray, V. Morchshakov, K. Barner, I.O. Troyanchuk, H. Nakamura, T. Kohara, G.Y. Liu, G.H. Rao, Phys. Rev. B 69 (2004) 064424.  
[48] T. Kimura, A. Asamitsu, Y. Tomioka, Y. Tokura, Phys. Rev. Lett. 79 (1997) 3720.  
[49] **A. Vlădescu**, S. Mican, C. Himcinschi, R. Tetean, JOURNAL OF OPTOELECTRONICS AND ADVANCED MATERIALS, Vol. 13, No. 3, March 2011, p. 263 – 267  
[50] K.W.Zhou, Y.H.Zhuang, J.Q.Li, J.Q.Deng, Q.M.Zhu, Solid State Commun. 137, 275 (2006).

## List of Publications

1. Deac I. G.; **Vlădescu A.**; Balasz, I., Tunyagi, A.; Tetean, R.  
*Low Temperature Magnetic Properties of  $Pr_{0.7}(Ca,Sr)_{0.3}CoO_3$  Oxides*  
ACTA. PHYS. POL. A Vol.: 120 Issue: 2 Pag.: 306-310 (2011)
2. Deac I. G.; Andreica D.; Balasz I.; **Vlădescu A.**, Dudric R.; Tetean, R.  
 *$\mu$ SR Investigation of magnetic phases in  $R_{1-x}Sr_xCoO_3$  oxides ( $R=Pr, Nd$ )*  
PHYSICA B. Volume: 406 Issue: 14 Pages: 2795-2800
3. **Vlădescu A.**; Mican S.; Himcinschi C.; Tetean, R.  
*Magnetocaloric effect in  $La_{1.2}R_{0.2}Ca_{1.6}Mn_2O_7$  compounds*  
J. OPTOELECTRON ADV. M. Volume: 13 Issue: 2-4 Pages: 263-267 (2011)
4. Deac IG, **Vlădescu A.**; Balasz I; Tunyagi A; Tetean R  
*Electrical and magnetic properties of transition metal oxides  $Ln_{1-x}A_xMO_3$  ( $Ln = Pr, Nd; A = Ca, Sr; M = Mn, Co$ )*  
J. OPTOELECTRON ADV. M. Vol.: 12 Issue: 8 Pag.: 1818-1824 (2010)
5. Pascuta P., **Vlădescu A.**, Borodi G., Culea E., Tetean R.  
*Structural and magnetic properties of zinc ferrite incorporated in amorphous matrix,*  
Ceramic International, 37, 3343-3349, 2011
6. Pascuta P., **Vlădescu A.**, Borodi G., Culea E., Tetean R.  
*Synthesis, structural and magnetic characterization of iron-zinc-borate glass ceramics containing nanocrystalline ferrite*  
J.Mater Sci: Mater Electron DOI 10.1007/s10854-011-0444-4

7. Deac IG; **Vlădescu A.**; Balasz I; Tunyagi A; Tetean R.  
*Electrical and magnetic behavior of transition metal oxides  $Ln_{0.7}A_{0.3}TMO_3$ ,  $Ln = La, Pr$ ;  
 $A = Ca, Sr$  AND  $TM = Mn, Co$*   
**INT J MOD PHYS B** Volume: 24 Issue: 6-7 Pages: 762-769
  
8. Deac IG, Tetean R, Balasz I, Andreica D, **Vlădescu A**, Dudric R, Tunyagi AR and Burzo E.  
*Magnetic transitions in the perovskites  $Pr_{1-x}Sr_xCoO_3$*   
J. Phys.: Conf. Ser. **200** 052003
  
9. Iosif G. Deac, **A. V. Vladescu**  
*Glassy magnetic behaviour in the perovskite transition metal oxides  $Pr_{0.7}Ca_{0.3}TMO_3$   
( $TM = Mn, Co$ )* STUDIA UBB PHYSICA, LV, 1, 2010